Numerical investigation of initial stage of bubble rise

M Liu, L Tan*, S L Cao and B B Wang

State Key Laboratory of Hydroscience and Engineering, Tsinghua University, Beijing 100084, China

Corresponding author E-Mail: tanlei@mail.tsinghua.edu.cn

Abstract. The numerical investigation has been carried out on the initial stage of bubble free rise in still water. The simulation and analysis focus on the separation behavior of air bubbles. The Large Eddy Simulation (LES) and Volume-of-Fluid (VOF) methods are applied as the turbulence model and multiphase model, respectively. The bubble behavior and flow field are analysed to reveal the mechanism of bubble separation. The predicted results show that there exists a funnel shape air gathering on the injection hole of water tank, and the air bubbles are separated from the upper part gradually. The separation behavior of air bubble results from the back flow induced by vortex structure. The strength difference of vortex in both sides is the major cause of zigzag motions of streamlines and bubbles.

1. Introduction

Multiphase flow is an important phenomenon that appears in many natural environment and industrial process. Bubble rising through water is typical multiphase flow, which is related to many practical examples, such as gas bubbles in oil wells and steam rising in boiler tube. The bubble rise in viscous liquid is a complex flow due to the growth, deformation, and collapse of disperse bubbles, which always leads to complicated unsteady characteristics of velocity and pressure, and hence energy dissipations.

Due to the importance and complexity of bubble rising phenomenon, many investigations have focused on the subject to reveal flow mechanisms. Brucker [1] researched the structure and dynamics of the wake of air bubbles rising by digital-particle-image-velocimetry and high-speed recording and found spiraling, zigzagging, and rocking motions during rising process. Ellingsen [2] experimentally studied an air bubble rising in still water. It was found that two unsteady modes with same the same frequency were involved in bubble dynamics. Vries [3] investigated the wake structures behind bubbles at high Reynolds number. Experiment results showed that zig-zag rising bubbles had double-threaded wakes and bubbles would lose their wakes after collision on wall. Advanced measurement techniques such as Particle Image Velocimetry (PIV), Acoustic Doppler Velocimetry (ADV) and Laser Induced Fluorescence (LIF), have been introduced to the research of bubble rising. Sanada [4] compared the interaction effects of bubble in-chain and single bubble by means of PIV measurement. Observations of bubble trajectories indicated different path occurred at different bubble released frequency. Bubbles went through an almost identical trajectory at low released frequency, while at high frequency bubbles would be disturbed by leading bubbles. Wang [5] investigated the rise velocity of bubble in-chain in still water and with cross flow by ADV technique. A non-dimensional cross flow velocity was proposed to distinguish regimes of different interaction strength. Huang [6] discussed the differences in various aspects between contaminated system and clean system, including: mass transfer,

bubble motion and surrounding liquid motion. LIF technique was used to visualize the three-dimensional wake structure. The terminal velocity is a characteristics parameter to describe bubble rising. A theoretical model of terminal velocity was proposed by Tomiyama [7] based on experiment measurement of a single bubble rising through an infinite stagnant liquid. It was found that the major cause of widely scattered terminal velocity was initial shape. Other researchers [8] also focused on drag coefficient fluctuations of single bubble, which was significantly related to terminal velocity.

With the rapid development of computer science, Computational Fluid Dynamics (CFD) has been applied in the investigations to obtain detailed data of flow field. In the multiphase case of bubble rising, the gas phase is always discrete while the liquid phase is continuous. To capture the liquid-gas interphase, the volume of fluid (VOF) method is commonly employed in the numerical simulations. Chen [9] simulated the rise and deformation of gas bubbles in a cylinder space by means of VOF method, and the simulation results agreed with experiments. Ruzicka [10] investigated the dynamic behavior of spherical gas bubbles in-chain by modeling major forces, including buoyancy, viscous drag, and inviscid inertia force. Sussman [11] combined the Level Set method and Volume-of-Fluid method to study three-dimensional axisymmetric two-phase flows, and the calculated results were more accurate than either single method alone. Other improved numerical algorithms have also been proposed and proved to be effective, such as front tracking method [12, 13]. Kozelkov [14] analyzed the dynamic behavior of single air bubble rising by solving three-dimensional Navier-Stokes equations with tracking of gas-liquid interface, and the predicted velocities were in good agreement of experiment data. VOF method is a typical Eulerian-Eulerian multiphase model, and Eulerian-Lagrangian multiphase model was also applied in the simulation of bubble free rise. Fraga [15] studied the influence of bubble size, diffuser width, and flow rate on bubble behavior based on Large Eddy Simulation (LES) and Eulerian-Lagrangian multiphase model.

Despite various numerical studies on free bubble rise in still water, the LES and VOF method has barely combined in the researches. In the current investigations, these two methods are employed to simulate gas-liquid flow on the initial stage of rising, and the predicted flow field are analyzed.

2. Mathematical Model

2.1. LES method

By performing filtering operation to the mass and momentum conservation equations in the Cartesian coordinates, the following filtered equations based on LES method can be derived:

$$\frac{\partial \rho_m}{\partial t}+\frac{\partial\left(\rho_m \bar{u}_j\right)}{\partial x_j}=0 \tag{1}$$

$$\frac{\partial\left(\rho_m \bar{u}_i\right)}{\partial t}+\frac{\partial\left(\rho_m \bar{u}_i \bar{u}_j\right)}{\partial x_j}=-\frac{\partial \bar{p}}{\partial x_i}+\frac{\partial}{\partial x_j}\left(\mu_m \frac{\partial \bar{u}_i}{\partial x_j}\right)-\rho \frac{\partial \tau_{ij}}{\partial x_j} \tag{2}$$

where ρ, u, p and μ are density, velocity, pressure and dynamic viscosity, respectively; $\rho_m=\rho_l\alpha_l+\rho_a\alpha_a$, $\mu_m=\mu_l\alpha_l+\mu_a\alpha_a$, subscripts l, a, m denote the liquid phase, air phase, and the mixture phase respectively; α_l and α_a are liquid and air volume fraction; the over-bar denote filtered quantity, τ_{ij} are the subgrid-scale (SGS) stresses, which is defined by:

$$\tau_{ij}=\overline{u_i u_j}-\bar{u}_i \bar{u}_j \tag{3}$$

The eddy viscosity model is applied to model the SGS stresses, which are calculated by:

$$\tau_{ij} = -2\mu_t \overline{S_{ij}} + \frac{1}{3}\delta_{ij}\tau_{kk} \tag{4}$$

where $\overline{S_{ij}}$ is strain rate tensor, μ_t is the subgrid-scale turbulent viscosity which needs to be closed. The Wall Adapting Local Eddy Viscosity (WALE) model is employed in current research, the subgrid-scale turbulent viscosity μ_t is obtained by:

$$\mu_t = \rho_m L_s^2 \frac{\left(S_{ij}^d S_{ij}^d\right)^{\frac{3}{2}}}{\left(\overline{S}_{ij}\overline{S}_{ij}\right)^{\frac{5}{2}} + \left(S_{ij}^d S_{ij}^d\right)^{\frac{5}{4}}} \tag{5}$$

$$S_{ij}^d = \frac{1}{2}\left(\left(\frac{\partial \overline{u}_i}{\partial x_j}\right)^2 + \left(\frac{\partial \overline{u}_j}{\partial x_i}\right)^2\right) - \frac{1}{3}\delta_{ij}\left(\frac{\partial \overline{u}_k}{\partial x_k}\right)^2 \tag{6}$$

$$L_s = \min\left(kd, C_s V^{\frac{1}{3}}\right) \tag{7}$$

where L_s is mixing length of subgrid scales, distance to the closest wall, volume of the computational cell, respectively. k and C_s are von Karman constant and WALE constant respectively, and C_s is equal to 0.5 according to calibrations by the freely decaying isotropic homogeneous turbulence [16].

2.2. VOF method

The VOF method is employed to capture the volume fraction of each fluid. In the current research including air and liquid water, the equation of volume fraction has the following form:

$$\frac{\partial}{\partial t}\left(\alpha_a \rho_a\right) + \nabla \cdot \left(\alpha_a \rho_a v_j\right) = 0 \tag{8}$$

3. Numerical method and settings

The computational domain consists of a water tank of 800 mm height. The cross section is a square of 60 mm, as shown in figure 1. At initial time, the water tank is filled with water, and then air is injected into water tank through the injection hole of 4 mm at the bottom. The structural hexahedron mesh are generated by ICEM 14.5 with special refinement near tank bottom. The technique of O-block is applied around the hole to improve mesh quality. The mesh of 2376000 elements are used in the following investigations.

Commercial Computational Fluid Dynamics (CFD) code ANSYS Fluent 17.0 is employed to solve the three-dimensional multiphase turbulent flow, based on LES method with WALE SGS model and explicit VOF method. The numerical settings are in coincidence with the experiment measurement of Wang [5]. The boundary includes an imposed velocity at the hole, a no-slip wall condition at other part at tank bottom, and a static pressure at tank top. The symmetry conditions are set at vertical wall surface to simulate infinite flow field. The unsteady time step is set as 1×10^{-4} to capture bubble trajectory.

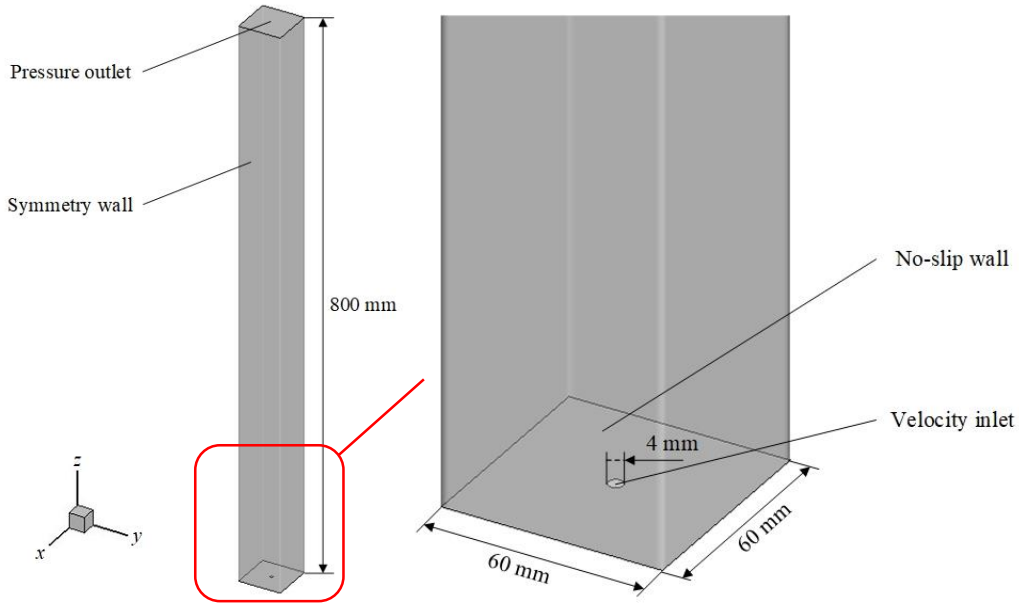

Figure 1. Computational domain.

4. Result and discussion

4.1. Bubble behavior

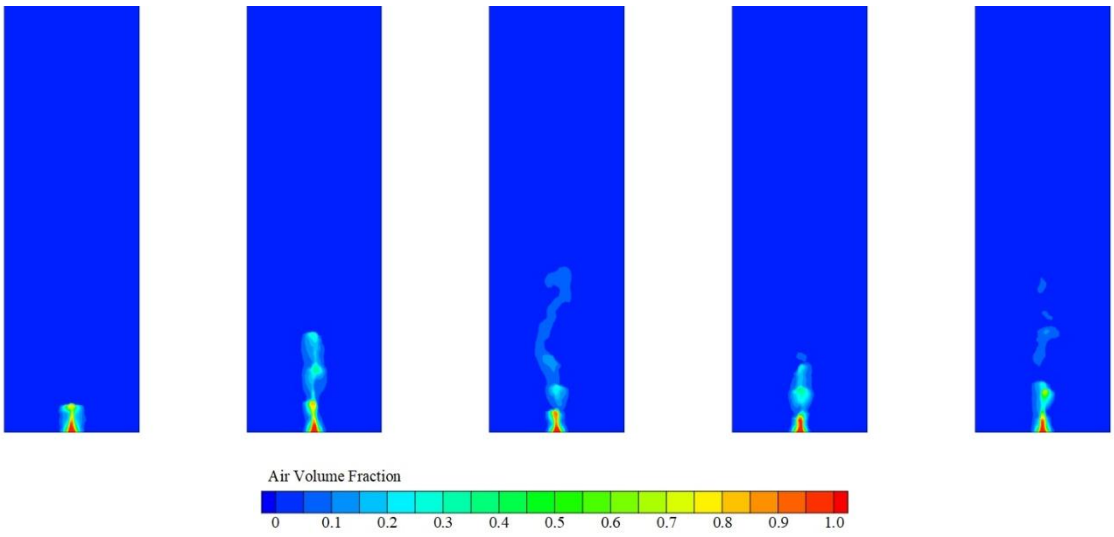

(a) t = 0.2 s (b) t = 0.4 s (c) t = 0.6 s (d) t = 0.8 s (e) t = 1.0 s

Figure 2. Time evolution of air volume fraction.

In the current research, the volume flow rate of air is 76.2 ml/min, and the water in tank is still, which corresponding to conditions of case-T (Q11) in Wang's measurement [5]. Totally one seconds are calculated to simulate the initial stage of free rise process in still water. Figure 2 shows the time evolution of vapor volume fraction on middle plane in *y*-direction with a time interval of 0.2 s. A gathering of air with high volume fraction exists near injection hole. The air gathering of high volume fraction appears in a shape of funnel. The bottom part of air gathering is almost stable, and the air bubble is separated from the upper part continuously.

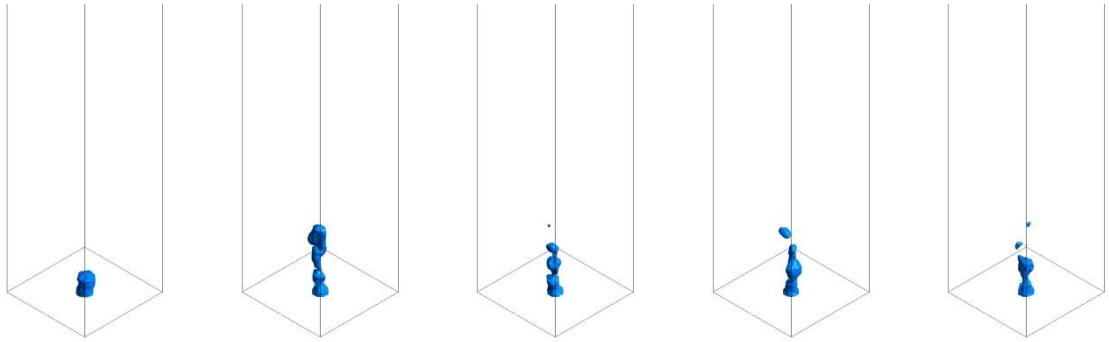

(a) t = 0.2 s (b) t = 0.4 s (c) t = 0.6 s (d) t = 0.8 s (e) t = 1.0 s

Figure 3. Isosurfaces of 10% volume fraction.

From figure 2(a) to figure 2(c), the stage of bubble inception can be observed. The region of air develops upwards from 0.2 s to 0.4 s and presents in a chain shape. The air volume fraction of this developed region is relatively lower than funnel shape region on the hole. Two potential bubbles appear in chain, as shown in figure 2(b), which indicates that two individual bubbles will be separated from the air gathering. Finally, the air bubble sheds from the funnel shape gathering and starts to rise freely, as shown in figure 3(d). Once the bubble is separated, the shape of air gathering on the hole changes from funnel to cone. Later, the air gathering comes back to the shape of funnel again and prepares for the formation of next air bubble.

It is of great importance to capture the shape of air bubble. Previous numerical investigations about cavitaing flow shows that the isosurfaces of 10% vapor volume fraction can describe best the real cavity shape [17, 18]. In the current research, it is found that this method is still appropriate for air-liquid two-phase flow. Figure 3 shows the isosurface of 10% vapor volume fraction. The phenomenon of bubble in-chain can be observed.

4.2. Flow field

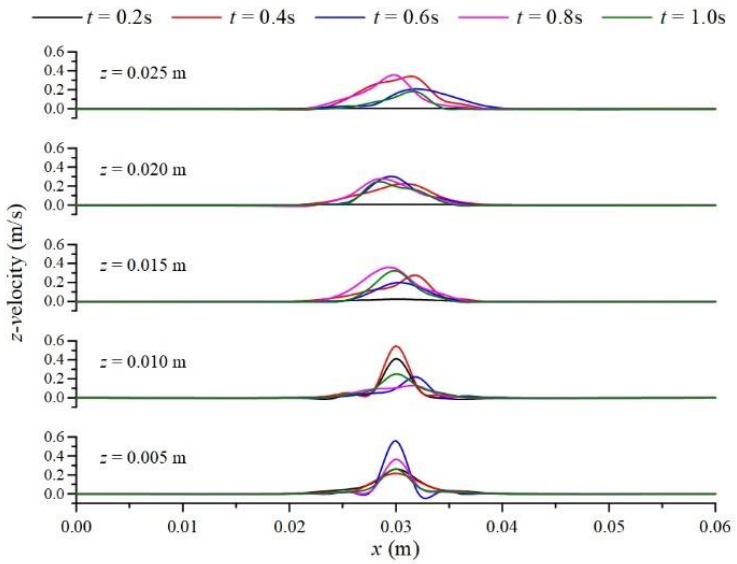

Figure 4. Velocity distribution.

In order to investigate velocity field during bubble inception, the distribution of z-velocity on the middle plane in y-direction at different height are shown in figure 4. Main flow occurs in the range

from x = 0.02 m to x = 0.04 m. The peak value of z-velocity gradually decreases with the rise of height, from nearly 0.6 m/s (at the height of 0.005 m and 0.0010 m) to no more than 0.4 m/s (at the height of 0.015 m, 0.02 m and 0.025 m). Meanwhile, the velocity distribution becomes more uniform and the range of main flow becomes larger as the height increases. At different time, the distribution of velocity also varies. During initial time (from t = 0 s to t = 0.6 s), sharp variation at different height on one snapshot can be observed. While when time exceeds 0.8 s, the quantity of z-velocity slightly changes at different height. This phenomenon indicates that the dynamic behavior of bubble flow has become stable approximately after 0.8 s. A significant back flow exists at the height of 0.005 m, and it is related to the throat of funnel and bubble separation.

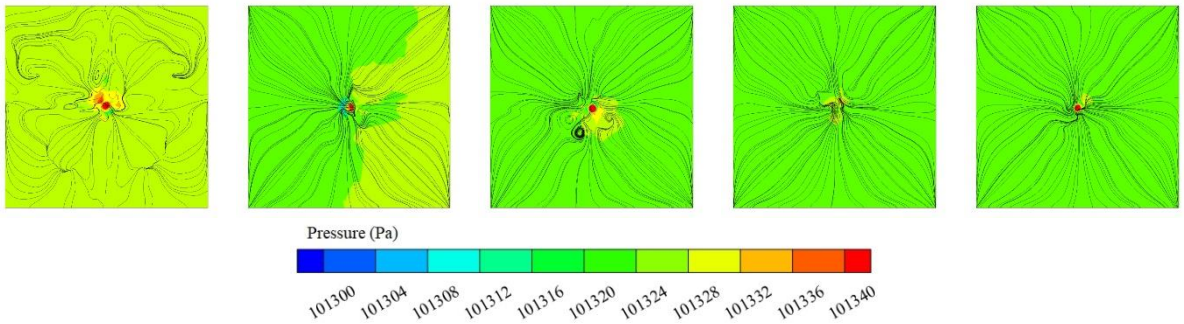

(a) t = 0.2 s (b) t = 0.4 s (c) t = 0.6 s (d) t = 0.8 s (e) t = 1.0 s

Figure 5. Distribution of pressure and surface streamlines on z = 0.01 m.

Because of the importance of velocity distribution in the plane of z = 0.01 m, the pressure distribution and surface streamline on the plane are illustrated in figure 5. The pressure distribution far from the injection hole is relatively uniform, while in the region above the hole, the pressure is significantly higher than other regions due to the effect of air injection. This high pressure region extends to adjacent area and results in vortex structure, as shown in figure 5(3). The vortex structure are coincidence with the asymmetrical velocity distribution in figure 4.

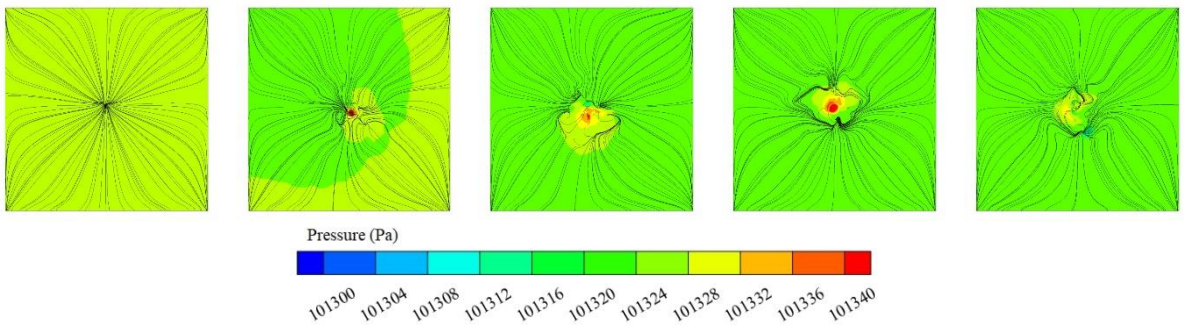

(a) t = 0.2 s (b) t = 0.4 s (c) t = 0.6 s (d) t = 0.8 s (e) t = 1.0 s

Figure 6. Distribution of pressure and surface streamlines on z = 0.02 m.

The plane of z = 0.02 m is another representative plane where bubble separation occurs. Figure 6 illustrates the pressure distribution and surface streamlines on the plane. At t = 0.2 s, the distribution of pressure and streamlines are almost axisymmetric because the air gathering has not reached the height of 0.02 m. With the growth of air gathering, the flow field around the hole becomes unstable. High pressure region appears with vortex structure, as shown in figure 6(c) and figure 6(d). In figure 6(e), after the air bubble is separated from the air gathering totally, the pressure on the plane decreases into a relatively low level.

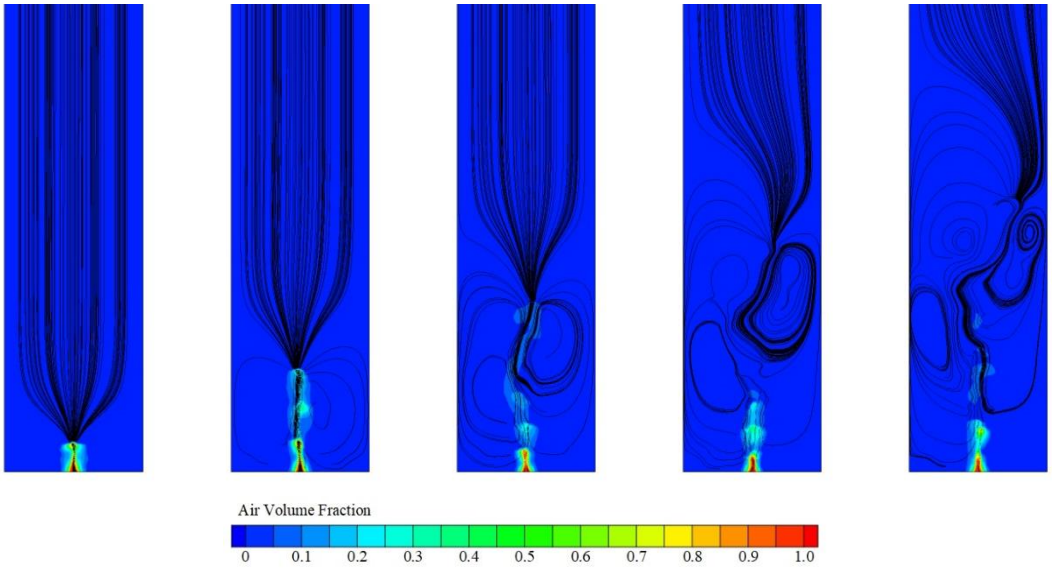

(a) t = 0.2 s (b) t = 0.4 s (c) t = 0.6 s (d) t = 0.8 s (e) t = 1.0 s

Figure 7. Distribution of air volume fraction and surface streamlines on middle plane

The figure 5 and figure 6 indicates that the bubble separation in the initial stage of rising is significantly related to the vortex structure. To reveal the mechanism of bubble separation, the distribution of air volume fraction and surface streamlines are illustrated on the middle plane in *y*-direction, as shown in figure 7. The flow field is almost axisymmetric at initial time. Then, with the volume increasing of air gathering, two vortex structure rotating in opposite directions appears at both sides of the central line. The vortex structure starts from the top bubble and ends at the upper part of funnel-shape air gathering. The vortex in the right side is somewhat larger than that in the left side, and this difference of vortices strength leads to the deviation of streamlines towards the left side, as shown in figure 7(3). The back flow induced by vortex structure is the major cause of bubble separation. Subsequently, the left deviation of streamline leads to a zigzag motion with forward right deviation and subsequent right deviation, as shown in figure 7(4) and figure 7(5). This zigzag streamlines are the reason of zigzag bubble trajectories which have been reported by previous researchers. Due to the right deviation of forward streamlines, there appears another vortex in the left side.

5. Conclusion

The numerical investigation are carried to study the initial stage of bubble free rise in still water with emphasize on the separation behavior of air bubbles. The LES method and VOF method are employed to solve the three-dimensional turbulent air-liquid two-phase flow. The bubble behavior and flow field are analyzed according to simulation results, and the following conclusions can be drawn:

- Due to the air injection through hole at the bottom of water tank, there exists an air gathering on the hole, which presents in a shape of funnel. The air bubbles are separated from the upper part of funnel shape gathering gradually.
- The separation behavior of air bubble is related to the vortex structure. The vortices in the both side of central lines rotates in the opposite direction, and induces the back flow which promotes bubble separation. The difference of vortex strength leads to the zigzag motion of streamlines.

Acknowledgments

This work has been supported by the National Natural Science Foundation of China [Grant number 51741906], the Tsinghua University Initiative Scientific Research Program [Grant number 2014z21041], and the Beijing Natural Science Foundation [Grant number 3164045].

References

[1] Brucker C 1999 *Phys Fluids* **11** 1781-96
[2] Ellingsen K, and Risso F 2001 *J Fluid Mech* **440** 235-69
[3] de Vries A, Biesheuvel A, and van Wijngaarden L 2002 *Int J Multiphas Flow* **28** 1823-35
[4] Sanada T, Watanabe M, Fukano T, and Kariyasaki A 2005 *Chem Eng Sci* **60** 4886-4900
[5] Wang B, and Socolofsky S 2015 *Phys Fluids* **27** 103301
[6] Huang J, and Saito T 2017 *Chem Eng Sci* **170** 105-15
[7] Tomiyama A, Celata G, Hosokawa S, and Yoshida S 2002 *Int J Multiphas Flow* **28** 1497-1519
[8] Yan X, Jia Y, Wang L, and Cao Y 2017 *Chem Eng J* **316** 553-562
[9] Chen L, Garimella S, Reizes J, and Leonardi E 1999 *J Fluid Mech* **387** 61-96
[10] Ruzicka 2000 *Int J Multiphas Flow* **26** 1141-81
[11] Sussman M, and Puckett E 2000 *J Comput Phys* **162** 301-37
[12] Hua J, and Lou J 2007 *J Comput Phys* **222** 769-95
[13] Hua J, Stene J, and Lin P 2008 *J Comput Phys* **227** 3358-82
[14] Kozelkov A, Kurkin A, Kurulin V, Lashkin S, Tarasova N, and Tyatyushkina E 2016 *Fluid Dynam* **6** 709-21
[15] Frage B, and Stoesser T 2016 J Geophys Res-Oceans 121
[16] Nicoud F, and Ducros F 1999 *Flow Turbul Combust* **62** 183-200
[17] Dular M, Bachert R, Stoffel B, and Sirok B 2005 *Eur J Mech B-Fluid* **24** 522-538
[18] Tan L, Zhu B, Cao S, Wang Y, and Wang B 2014 *Energies* **7** 1050-65